Combining machine learning and SMILEs to classify, better understand, and project changes in ENSO events

Nicola Maher[1,2], Thibault P. Tabarin[3], and Sebastian Milinski[1,4,5]

[1]Max Planck Institute for Meteorology, Hamburg, Germany
[2]Cooperative Institute for Research in Environmental Sciences (CIRES) and Department of Atmospheric and Oceanic Sciences (ATOC), University of Colorado at Boulder, Boulder, CO 80309, USA
[3]Freelancer, Boulder, CO 80303, USA
[4]Climate and Global Dynamics Division, National Center for Atmospheric Research, Boulder, CO 80307, USA
[5]Cooperative Programs for the Advancement of Earth System Science, University Corporation for Atmospheric Research, Boulder, CO 80307, USA

Correspondence: Nicola Maher (nicola.maher@colorado.edu)

Abstract.

The El Niño Southern Oscillation (ENSO) occurs in three phases: neutral, warm (El Niño) and cool (La Niña). While classifying El Niño and La Niña is relatively straightforward, El Niño events can be broadly classified into two types: Central Pacific (CP) and Eastern Pacific (EP). Differentiating between CP and EP events is currently dependent on both the method and observational dataset used. In this study, we create a new classification scheme using supervised machine learning trained on 18 observational and reanalysis products. This builds on previous work by identifying classes of events using the temporal evolution of sea surface temperature in multiple regions across the tropical Pacific. By applying this new classifier to seven single model initial-condition large ensembles (SMILEs) we investigate both the internal variability and forced changes in each type of ENSO event, where events identified behave similarly to those observed. It is currently debated whether the observed increase in the frequency of CP events after the late 1970s is due to climate change. We found it to be within the range of internal variability in the SMILEs for trends after 1950, but not for the full observed period (1896 onwards). When considering future changes, we do not project a change in CP frequency or amplitude under a strong warming scenario (RCP8.5/SSP370) and we find model differences in EP El Niño and La Niña frequency and amplitude projections. Finally, we find that models show differences in projected precipitation and SST pattern changes for each event type that do not seem to be linked to the Pacific mean state SST change, although the SST and precipitation changes in individual SMILEs are linked. Our work demonstrates the value of combining machine learning with climate models, and highlights the need to use SMILEs when evaluating ENSO in climate models due to the large spread of results found within a single model due to internal variability alone.

1 Introduction

Understanding El Niño Southern Oscillation (ENSO) diversity is important due to the differing teleconnections and impacts of different types of events (e.g. Capotondi et al., 2020, and refs therein). ENSO occurs in three phases: neutral, La Niña, and El

Niño. While El Niño events occur with a wide range of spatial structures (Giese and Ray, 2011) they can be broadly classified into two types, which differ in evolution, strength and spatial structure (e.g. Capotondi et al., 2015, 2020). These are eastern Pacific (EP) El Niños, and central Pacific (CP) El Niños. EP El Niños have warm sea surface temperature (SST) anomalies located in the eastern equatorial Pacific, typically attached to the coastline of South America, while for CP El Niños SST, wind and subsurface anomalies are confined to the central Pacific (Kao and Yu, 2009). EP events tend to appear in the far east Pacific and move westward, with CP events generally appearing in the eastern subtropics and central Pacific (Kao and Yu, 2009; Yeh et al., 2014; Capotondi et al., 2015). EP events occur from weak to extremely strong in amplitude, while CP events tend to be on the weaker side (e.g. Capotondi et al., 2020). In this study we use supervised machine learning techniques to create a new classification scheme.

There is ongoing debate about the cause of an observed increase in the frequency of CP events after the late 1970s (An and Wang, 2000). This was initially attributed to increased greenhouse gas forcing (Yeh et al., 2009). Other studies then suggested that multi-decadal modulation of CP frequency by internal variability can explain this increase (McPhaden et al., 2011; Newman et al., 2011; Yeh et al., 2011; Pascolini-Campbell et al., 2015). However, a recent study again suggested that this observed increase can be linked to greenhouse gas forcing (Liu et al., 2017). Additionally, paleoclimate records have shown that the current ratio of CP to EP El Niños is unusual in a multi-century context (Freund et al., 2019). Freund et al. (2019) use corals from 27 seasonally resolved networks and find that compared to the last 4 centuries the recent 30-year period includes fewer, but more extreme EP El Niños and an unprecedented ratio of CP to EP El Niños compared to the rest of the record. It is currently unresolved why these past changes seen in the paleoclimate record occurred.

Whether both the frequency and amplitude of EP and CP events will change in the future is also strongly debated. Multiple studies agree that projections are inconsistent across CMIP5 models (Ham et al., 2015; Chen et al., 2017b; Xu et al., 2017; Lemmon and Karnauskas, 2019). These differences are suggested to be related to the central pacific zonal SST gradient (Wang et al., 2019). When subsetting for models that represent ENSO well, studies find an increase in EP variability (Cai et al., 2018, 2021). However, when using single model initial-condition large ensembles (SMILEs), models are again found to differ in their projections (Ng et al., 2021). ENSO precipitation projections are more robust across all models with multiple studies projecting an increase in ENSO related precipitation variability under strong warming scenarios (Power et al., 2013; Cai et al., 2014; Chung et al., 2014; Watanabe et al., 2014; Huang and Xie, 2015; Yun et al., 2021).

While there is a wealth of literature investigating ENSO, previous work has highlighted that due to its high variability longer equilibrated runs or SMILEs are needed to truly understand our observations of ENSO and to project future changes (Wittenberg, 2009; Maher et al., 2018; Milinski et al., 2020). Two separate studies show that two SMILEs cover the spread of ENSO projections in CMIP5 models for both traditional ENSO indicies (Maher et al., 2018) and EP and CP events (Ng et al., 2021). This indicates that internal variability can explain a large fraction of the inter-model spread previously attributed to model differences. These results highlight the utility of SMILEs, which provide many realisations of the earth system and allow scientists to investigate both the climate change signal as well as inherently complex and noisy systems such as ENSO (Maher et al., 2018).

Previous studies have used varying methods to classify El Niños into EP and CP events, but are limited by uncertainty in both the observed data and the classification method. Pascolini-Campbell et al. (2015) summarize nine classification schemes (Ashok et al., 2007; Hendon et al., 2009; Kao and Yu, 2009; Kim et al., 2009; Kug et al., 2009; Ren and Jin, 2011; Takahashi et al., 2011; Yeh et al., 2009; Yu and Kim, 2010) applied to five different SST products and show that event classification is dependent on both the index and dataset used. They identify events that appear with greatest convergence across indexes and datasets to provide the most robust classification of observations to date. Such classification using multiple SST products can now be automated using machine learning, which has the additional advantage of using multiple parameters across many dimensions to identify events. This technique provides potential to create a more complete classifier than previous studies, where classification schemes have focused on single metrics with defined thresholds or comparing multiple schemes and products by hand (Pascolini-Campbell et al., 2015).

Machine learning techniques such as classification are becoming more commonly utilised in the geosciences. The key challenges in applying machine learning in this field come from the difficulty in ground truthing data, interpreting physical results, auto-correlation at both spatial and temporal scales, noisy data with gaps that is taken at multiple resolutions and scales, as well as data that is uncertain, sparse, and intermittent (Gil et al., 2018; Karpatne et al., 2019; Reichstein et al., 2019). Machine learning, however, also provides new opportunities in the geosciences particularly when using climate models where large coherent datasets exist (Barnes et al., 2020, 2019; Toms et al., 2020). Studies have begun to apply such techniques to ENSO research, for example using unsupervised learning and clustering algorithms to identify different types of ENSO event (Wang et al., 2019; Johnson, 2013) and to more reliably predict ENSO (Ham et al., 2019; Guo et al., 2020). However, no studies to date have used supervised learning combined with observations to investigate ENSO. In this study, we use supervised machine learning to build a new ENSO classifier. We then apply this classifier to climate models to identify events that resemble those found in the real world. This is relevant as we wish to study events similar to those that we observe.

The aims of this paper are twofold. First, we create a new classifier using supervised machine learning combined with 18 observational and reanalysis products. This classifier has the advantage that it can learn both the spatial and temporal evolution of different events unlike previous studies that rely on pre-defined metrics and comparing multiple methods and products by hand. Second, we apply the classifier to seven SMILEs to answer three questions. One, can SMILEs capture the observed CP and EP El Niños, and La Niñas? Two, can the observed increase in frequency of CP El Niños be explained by internal variability and what does this imply for future projections? Three, do we project forced changes in the amplitude, SST and precipitation patterns of each event type? By using this classifier combined with SMILEs we can now better understand observations and projections of ENSO in the light of internal variability.

2   Creating the classifier

The purpose of a classifier is to assign a class to an event. In this paper our intent is to label each year with one of four event types: central Pacific (CP) El Niño, eastern Pacific (EP) El Niño , La Niña (LN), and neutral (NE). We use supervised learning in this study. Supervised learning algorithms use a labelled dataset to train a classifier (e.g. observations where a class

is already assigned to each individual year from previous studies). Then this classifier can be applied to unlabelled data (e.g.
climate model output where no class has yet been assigned for each individual year).

There are 7 steps to creating a machine learning classifier:

1. **Data Collection**: the quality and quantity of the data used dictates how well the classifier performs

2. **Data Preparation**: choosing which features (individual variables) from the dataset will be given to the classifier, pre-processing the data, as well as well as splitting the data into training and evaluation sets, labelling the data

3. **Choosing a classifier**: different algorithms are suited to different purposes and data types

4. **Training the classifier**: using the training set to train the classification algorithm

5. **Evaluating the classifier**: using the evaluation set to assess how the classifier performs, one must define an appropriate scoring metric fit for purpose

6. **Hyper-parameter tuning**: tuning the classification algorithm parameters for better performance

7. **Prediction**: using the classifier to make predictions from other datasets, at this point we have a tool that will allow us to classify and investigate ENSO events in climate model output

The following sections provide a description of the steps followed in this study. These steps are merged into sections as some steps are performed in unison and/or iterated through.

2.1 Data collection and preparation

Steps 1 & 2 data collection and data preparation are outlined in this section. In this study we use SST data due to its good temporal and spatial coverage over the tropical Pacific Ocean. We choose not to include other variables due to their shorter record lengths. Additionally, by using SST alone we can independently assess the projected precipitation response in climate models during the prediction phase. We label each year of the observational dataset as EP, CP, LN or NE using results from previous studies (Table 1). Here, we use the most robust set of labels available for CP from Pascolini-Campbell et al. (2015).

Machine learning classifiers work best with large amounts of training and testing data. Unfortunately, although for an observed climate variable SST has a relatively long record, there are only 124 years of data, which include only 14 CP events and 20 EP events (Table 1). This is an inherent problem when using climate data that has been highlighted in much of the literature (e.g. Reichstein et al., 2019). As the data is time-dependent we cannot easily acquire more data. Due to the spatial correlations within the dataset typical machine learning augmentation methods, which would be used to artificially create additional data, are not appropriate. Instead in this study we use an unconventional augmentation method where we opt to use 18 observational and reanalysis products (Table S1). Each product includes the same events with the same labels, however due to observational uncertainty, infilling methods, and the use of reanalysis models, the SST patterns are different (e.g. Deser et al., 2010; Pascolini-Campbell et al., 2015; Huang et al., 2018). This unconventional data augmentation takes into account observational

4

uncertainty in addition to effectively augmenting the data we have to use in this study. Before training the classifier we create anomalies by detrending the data (using a third order polynomial) and removing the seasonal cycle (mean of each month over the entire time-series after detrending).

The next step in the data preparation process is to identify which features to use in the study. While La Niña, neutral and El Niño events are fairly easy to define, separating El Niño events into CP and EP classes can be difficult. Previous studies have identified that the Pacific SST in the predefined niño boxes, the north Subtropical Pacific, and the evolution of SST over the event, are the most important features for separating the two types of El Niño (e.g. Rasmusson and Carpenter, 1982; Yu and Fang, 2018; Tseng et al., 2022). In this study we use the regions niño3E (5S-5N, 120-90W), niño3W (5S-5N, 120-150W), niño4E (5S-5N, 150-170W), niño4W (5S-5N, 170-200W), and niño1.2 (0-10N, 80-90W) in each month from June to March as individual features to train the classifier (i.e. 5 regions x 10 months = 50 features). We note that we tested multiple feature sets including varying regions in the tropical and north subtropical Pacific and different sets of months for performance (see Supplementary Information 2: Supplementary Methods), and chose this set due to its high performance in the evaluation phase.

In machine learning, part of the dataset is used for training, while the rest of the data is kept aside for evaluation of the classifier performance. In the following section when evaluating how the classifier performs we keep the HadISST observational dataset aside and use all other data in the training phase. This choice was made due to the limited number of events in the observed record, where splitting the data by event rather than dataset may result in the loss of events that are important to the training phase of the classification algorithm.

2.2 Choosing, training, evaluating, and tuning the classifier

Steps 3, 4, 5 & 6: choosing, training, evaluating and tuning the classifier are outlined in this section. We outline these steps together as we iterate through the different steps to find the best performing classifier. There are a suite of algorithms typically used in supervised learning classifiers. It is common practice to test all algorithms and see how they perform on a particular dataset, given they all have different strengths and weaknesses. The 9 algorithms tested in this study are: (1) nearest neighbours, (2) linear support vector machine, (3) radical basis function support vector machine, (4) decision tree, (5) neural network, (6) adaboost, (7) naive bayesian, (8) quadratic discriminant analysis, and (9) random forest. We use the python scikit-learn package (Pedregosa et al., 2011) to train each of these algorithms on our SST dataset. To evaluate which algorithms perform best we use four different scores.

The first is an accuracy score, which defines the number of correct predictions out of all predictions:

$$accuracy = \frac{TP + TN}{TP + TN + FP + FN} \tag{1}$$

where, TP are true positives, TN are true negatives, FP are false positives and FN are false negatives.

The second is a precision score for each of the event types (i) that we want to classify, which tells us the proportion of positive predictions that are correctly predicted:

$$\text{precision}_i(P-i) = \frac{TP_i}{TP_i + FP_i} \tag{2}$$

The third is a recall score for each of the event types (i) that we want to classify, which tells us the ability to correctly predict events compared to all positive predictions for that event:

$$\text{recall}_i(R-i) = \frac{TP_i}{TP_i+FN_i} \tag{3}$$

In all cases a score of 1 is best, while a score of 0 is worst. Accuracy, precision and recall scores are calculated on the evaluation dataset.

The fourth score is an accuracy cross validation score (CVS), which we use to test how robust our estimate is. Here, to test the classifier, the algorithm breaks the training data into n smaller datasets (in this study we use $n = 5$). For $n = 5$ the algorithm retrains the classifier using four of the five smaller datasets and tests on the fifth. We then obtain 5 accuracy scores which are averaged to give an estimate of the models performance. The cross validation score function in scikit-learn uses a KFold Stratification to split the data into these smaller datasets (Pedregosa et al., 2011). This is designed to keep the distribution of classes similar in each set and keep sets the same size.

In this study we are particularly interested in correctly identifying CP and EP events. This means that our algorithm must have high precision and recall scores for these two events. Based on the scores outlined above we evaluate all nine algorithms as well as ensemble classifiers that use multiple algorithms (see Supplementary Information 2: Supplementary Methods for details of all algorithms tested & Table 2). The best performing algorithm is an ensemble voting classifier, which utilises the strengths of three algorithms. These three algorithms are: a neural network, a random forest and a nearest neighbour. All three algorithms hyper-parameters are tuned for optimal performance (step 6) by evaluating the performance of the algorithm using the four scores listed above at varying values of each parameter. The three algorithms chosen, the hyper-parameters used after tuning and the scores after tuning, are shown in Table 2. The ensemble voting classifier uses the wisdom of the crowd, where all three algorithms vote to give the final outcome. We choose to use soft voting as it performs better in the evaluation stage (see Supplementary Information 2: Supplementary Methods). Soft voting predicts the class label based on the maximum of the sums of the predicted probabilities. Evaluation scores for the final classifier are found in Table 2. The slightly higher scores of this final classifier compared to each individual algorithm demonstrates the utility of combining three algorithms into a ensemble voting classifier. This final classifier correctly identifies 12/13 CP (note the 2019 CP events is not included in the test set), 20/20 EP, 22/26 LN and 64/64 NE events. Those not classified correctly are identified as NE.

Before using this classifier in step 7 to classify climate model output we perform one more set of tests based on the following limitation. A limitation of the original evaluation is the choice of training and evaluation sets. In our original choice, where we reserve HadISST for evaluation the same ENSO events are effectively included in both the training and evaluation sets. While this is the typical way to split the data when using data augmentation techniques, we additionally test the sensitivity to this choice. To do this we use the longer datasets (ERSSTv3b, ERSSTv4, ERSSTv5, HadISST, kaplan and COBE), which all cover the years 1896-2016 and separate the data so that each event is only included in the training or evaluation set.

To decide on how to separate the data into training and evaluation sets we use the python function train test split (Pedregosa et al., 2011) which shuffles the data then splits it into training and evaluation sets while preserving the percentages of events in both the training and testing data. We do this 10 separate times to get 10 sets of training and evaluation data and then compute

6

the scores shown in Table 3. We additionally complete this split 100 times and manually choose 10 data splits that take CP and EP (the classes with the lowest numbers of events) from across the time-series. This is done to ensure that not all events in the split come from the same part of the observational record. As observational data quality for SST is dependent on where in the record it occurs (e.g. lower quality early in the record) it is only appropriate to use data splits that include events across the entire record. We additionally test the algorithms with this split for HadISST alone to test the robustness of the result to using a single dataset.

We find that for all three data splits, there is a range of accuracy that depends on how the training and evaluation sets are constructed. We find that while the precision and recall scores can be quite low for some training/evaluation sets, other sets show high precision and recall, suggesting that the algorithm can perform reasonably well. This suggests that if the training and evaluation sets are constructed in an ineffective way and the training set does not include specific events vital for classification, then the testing result is poor. This is a problem that occurs due to our small data size. Based on these results when training the final classifier we choose to use all available data (including HadISST) so as not to lose information by excluding events. This final classifier is used in step 7 prediction to identify each type of ENSO event in climate model output.

2.3   Prediction

In machine learning, step 7: prediction refers to applying the trained classifier to other datasets. We apply the classifier trained on observed SST data to climate model output from 7 SMILEs. Besides having a large amount of events to classify, the advantage of using SMILEs is that we can assess how internal climate variability can affect what we observe in our single realisation of the world. In this study we use 5 SMILEs with CMIP5 forcing (historical and RCP8.5) and two SMILEs with CMIP6 forcing (historical and SSP370), all of which have more than 20 members (Table S2). We classify using the same features as in our training and evaluation data. We note that if large forced changes in the SST in the tropical Pacific occur under the future scenario the algorithm will have difficulty classifying future states as it is constrained by the information provided in the observational record. We assess changes in the SST and precipitation patters, amplitude and frequency of each event type. Amplitude is calculated as the November, December, January mean for the region 160E to 80W between 5N and 5S after the ensemble mean has been removed for each event in a single ensemble member taken as a running calculation along the time-series for 30-year periods. Frequency is calculated as the number of events in a single ensemble member per 30 years, taken as a running calculation along the time-series. We discuss the SMILE classification results in the following sections.

3   Application to SMILEs

3.1   Can SMILEs capture the observed CP, EP Niños and La Niñas?

We find CP and EP El Niños as well as La Niñas in all models, and identify known biases in their spatial patterns (Figure 1). The composite spatial patterns of SST in the peak ENSO season (November, December, January) for each different ENSO class in comparison to the HadISST composites are shown in Figure 1. CP events are visibly weaker than EP events in both

the SMILEs and observations. The known bias of ENSO where SST anomalies extend too far to the west is also clearly visible in all SMILEs, although it is more prominent in some models than others. The CSIRO model shows particularly strong SST biases, with a peak SST anomaly too far into the western Pacific.

The time-evolution of the SST anomalies is found to be different for each event type and appears to be important for classification (Figure 2). We find that the machine learning classifier does not just learn the SST pattern shown in Figure 1 and that CP events are weaker than EP events. It also correctly identifies the general pattern of how the SST anomalies evolve over the event, with CP El Niños initiated in the central Pacific, while EP El Niños begin in the eastern Pacific off the South American coastline and evolve into the central Pacific over the course of the event. This is supported by the fact that the classifier performs better when information about the time-evolution is included in the feature choice (see Supplementary Information 2.1: Choice of Features). The two CMIP6 models have smaller relative SST anomalies than observations, with the relative SST anomalies in the CMIP5 models more realistic in magnitude (assuming that the observed record is long enough to sample these events). Overall, all models bar CSIRO show both a realistic evolution of both EP and CP events as well as the differences between the two.

Due to the relatively short observational record, which has been shown to be insufficient to capture multi-decadal ENSO variability (Wittenberg, 2009; Maher et al., 2018; Milinski et al., 2020) we compare the range of frequencies found across each ensemble with observations (Table 4). We find that the observed frequencies of EP and CP El Niños and La Niña events are within the SMILE spread for most models. Individually, CanESM5 does not realistically capture EP or CP El Niño frequency, CSIRO has too low frequency of CP El Niño and La Niña events, and IPSL-CM6A has too low frequency of CP El Niño events. We also consider the pattern correlation between EP and CP events as compared to the observed pattern correlation to see how similar EP and CP Niños can look due to internal variability (Table 4). We find that the observed pattern correlation is always captured within the ensemble range of all SMILEs. However, individual ensemble members can have a large range of pattern correlations. This demonstrates that when using single realisations, a model may appear to not well represent the distinct EP and CP patterns by chance rather than due to model deficiencies.

Given climate models have known ENSO biases, particularly in the location of SST anomalies along the equator, we additionally classify by shifting the longitudes of the niño regions. This shift is defined as the difference in location between the maximum variability between 5N and 5S in the Pacific Ocean in the observations and the maximum variability in each individual SMILE (Table S5). We find that this does not significantly change the results in the previous paragraphs except for CSIRO frequency where EP Niños and La Niñas are now more realistically represented. This method additionally does not change the results for climate projections presented in the following sections (see Supplementary Information 3: Shifted niño regions).

When comparing these results to previous work, different studies identify different models as more realistic or able to represent different ENSO event types (e.g. Xu et al., 2017; Capotondi et al., 2020; Feng et al., 2020; Dieppois et al., 2021). From our comparison with observations we have assessed that most models capture the observed frequency of all event types and the correlation between the EP and CP Niño patterns, and demonstrate that previous work could find a variety of results for the same models due to the use of single realisations. We show that all models exhibit some SST bias, but that EP and CP events are

differentiated in the models for physically interpretable reasons. In this case the classifier identifies the spatial pattern, evolution, and amplitude of the different event types. However, just because some observed quantities fall within the SMILE range, does not mean each model does not have individual and differing biases in other quantities as presented by Bellenger et al. (2014); Karamperidou et al. (2017); Kohyama et al. (2017); Cai et al. (2018, 2021); Planton et al. (2021). ENSO complexity itself includes not only diversity in the form of EP and CP El Niños, but other metrics such as the transition, propagation and duration of events (e.g. Chen et al., 2017a; Timmermann et al., 2018; Fang and Yu, 2020). While the propagation of events is to some extent accounted for in the classifier with inclusion of the evolution over time, other metrics of ENSO complexity are also important in understanding ENSO events and could be considered using SMILEs in future work. Given the validation performed in this section we choose to include all models except CSIRO in the following analysis of projections. This is because CSIRO presents consistent strong biases in the pattern, evolution and frequency of events.

3.2 Can the observed increase in frequency of CP Niños be explained by internal variability and what does this imply for future projections?

The frequency of CP events was observed to increase after the 1970s (An and Wang, 2000) leading to the question of whether this was a forced change due to increasing greenhouse gas emissions (Yeh et al., 2009). In Figure 3 we show that the range of frequencies in CP (and EP and La Niña) events across a individual SMILE for a 30-year period is large. This implies that the observed increase in CP events could be due to internal variability alone, similar to Pascolini-Campbell et al. (2015) and Dieppois et al. (2021), who pointed out that CP frequency varies on multi-decadal timescales. This is the case in the SMILEs, when we consider a single ensemble member (Figure 3; green lines) there are periods where it sits higher and lower in the ensemble spread, demonstrating this multi-decadal variability. However, when we consider trends in individual ensemble members we get a different result. Observations show a increasing trend in frequency (defined as the number of events per 30years) of 7.78/100year for the entire observed period (1896-2019). The two models that cover the whole period do not capture this trend (max trend MPI-GE = 5.0, CanESM5=5.0). When we consider the shorter, better observed time period of 1950 onward the trend in observations increases to 8.4. However, in this case all models that cover the entire time period are able to capture this trend (max trend MPI-GE = 15.1, CESM-LE = 13.3, CanESM2 = 11.3, GFDL-ESM2M = 19.7, CanESM5 = 11.9). This suggests that the observed increase in CP could be due to internal variability alone, as the models capture the increase in CP events in the better observed period, however the inconsistencies in the earlier period also highlight potential model biases.

When assessing projected changes in frequency, we use a signal to noise ratio to identify changes. When the signal at any time point (ensemble mean at the time point minus the ensemble mean at the beginning of the time-series) is greater than the noise (standard deviation taken across the ensemble) we identify a *likely* projected change. When the signal is 1.645 or 2 times the noise these thresholds correspond to the *very likely* and *extremely likely*. CESM-LE and CanESM5 show a very and extremely likely increases in EP El Niño frequency respectively (Figure 3). CESM-LE projects a very likely increase in La Niña frequency with small likely decreases found at the end of the century for CanESM2 and GFDL-ESM2M. No model projects a significant change in CP frequency before the end of the century, where CanESM2 and GFDL-ESM2M project

285 a likely decrease in frequency. We note that large changes could be observed due to the considerable internal variability of these frequencies alone as demonstrated by the maximum and minimum frequencies, range of maximum and minimum trends across ensemble members, and the multi-decadal changes seen in the individual ensemble members (e.g. green line Figure 4). These results are interesting in the context of a paleoclimate study by Freund et al. (2019) who show that the current relative frequency of EP/CP events is unprecedented in the paleoclimate record. There are two possible reasons for the differences

290 between this study and our results. First, model biases may mean that the models cannot capture this shift correctly. Second, a shift in frequencies may have already occurred, after which we do not project further future shifts. This could be investigated further in future studies by applying this classification method to the last millennium long paleoclimate model simulations.

3.3   Do we project changes in the amplitude, SST and precipitation patterns of each event type?

When considering ENSO amplitude (November, December, January mean for the region 160E to 80W between 5N and 5S

295 after the ensemble mean has been removed for each event), similar to frequency we find that the range of amplitudes across each SMILE at any given time is quite large ($0.5 - 1.5^{o}C$) for each event type, with the difference between the maximum and minimum trends ranging from $0.1 - 2.5^{o}C/100yr$ across models (Figure 4). This agrees well with previous work that shows that ENSO amplitude is very variable in single realisations of climate models (e.g. Wittenberg, 2009; Maher et al., 2018; Ng et al., 2021; Dieppois et al., 2021). When projecting future changes, we find model disagreement on the forced change in EP

300 El Niño and La Niña amplitude (Figure 4). We find model agreement of no change in CP El Niño amplitude. We find a likely increase in the amplitude of EP events in CESM-LE and CanESM5, with likely and extremely likely decreases in GFDL-ESM2M and CanESM2 respectively. For La Niña events there is a likely decrease in CESM-LE and CanESM5, and very likely increases in CanESM2 and GFDL-ESM2M.

These results compare well to previous work, where El Niño amplitude was found to increase in CESM-LE, not change in

305 MPI-GE, and decrease in GFDL-ESM2M (Zheng et al., 2017; Haszpra et al., 2020; Maher et al., 2018, 2021; Ng et al., 2021). When partitioning amplitude changes into EP and CP events using different criteria for classification, Ng et al. (2021) found an increase in both EP and CP amplitude in CESM-LE and no change in MPI-GE. This agrees well with our results, although we do not see the increase in CP amplitude in CESM-LE, possibly due to the different time periods used and the relatively small magnitude of the change. Recently Cai et al. (2018) and Cai et al. (2021) showed that for CMIP5 and CMIP6 models

310 that represent some ENSO properties well, EP amplitude increases in most models. However, only two of the models they identified as able to represent ENSO well are included in our study (CESM-LE and GFDL-ESM2M) and they differ in sign (increasing amplitude in CESM-LE; decreasing amplitude in GFDL-ESM2M). This is in agreement with Cai et al. (2018) who also found decreasing amplitude in GFDL-ESM2M, which was an outlier in their study which used single ensemble members from CMIP5.

315 These model differences have been suggested to be related to changes in the zonal gradient of mean SST. Wang et al. (2019) suggest that an increase in the SST gradient results in an increase in the amplitude of strong basin wide El Niños, with a decrease leading to the a decrease in amplitude. Kohyama et al. (2017), however, suggest that a La Niña like warming pattern (i.e. the western Pacific warms more than the eastern Pacific, resulting in an increased zonal SST gradient), should result in a

decrease in ENSO amplitude as does Fredriksen et al. (2020). This result is in agreement with an observed decrease in tropical Pacific variability coupled with an increase in the trade winds and increase in thermocline tilt from 2000-2011 as compared to 1979-1999 (Hu et al., 2013). Beobide-Arsuaga et al. (2021) also find a weak negative correlation between the two quantities in CMIP5 and CMIP6 models. In our study two of the five SMILEs additionally show a weak negative relationship between these quantities, however three models (CESM-LE, CanESM2, and CanESM5) show no relationship (Figure S2a). We find no relationship between CP amplitude and the projected change in the zonal mean SST gradient (Figure S2b) consistent with Fredriksen et al. (2020).

We next plot the change in SST pattern for each event type for the period 2050-2099 as compared to 1950-1999 (Figure 5). We use detrended data to look at the changes in ENSO itself, outside of mean-state changes. We find similar pattern changes for EP and CP events, with the opposite change for La Niña events. The SST pattern change lacks agreement across the models. Potentially this is related to the mean state changes (Knutson et al., 1997; McPhaden et al., 2011; Hu et al., 2013; Kim et al., 2014; Kohyama et al., 2017; Wang et al., 2019; Beobide-Arsuaga et al., 2021), however the SST pattern change is different for CESM-LE and CanESM2, which have similar mean state changes suggesting that the relationship is more complicated than one simple metric.

Precipitation projections for each event type also show large differences between SMILEs (Figure 5 & 6). These projected pattern differences are, however, found to be linked to the projected SST patterns, with contours of increasing SST found to closely correspond to wetting, and decreasing SST to drying. This clarifies that ENSO changes in SST and precipitation are linked and that it is not possible to truly understand one without the other.

We compare the multi-ensemble mean patterns (Figure 6) to previous work using CMIP models. Xu et al. (2017) find similar strong cooling in RCP8.5 in the eastern Pacific for EP events, and some similarities of cooling in the eastern Pacific for CP events as well. For precipitation projections, EP events look similar to Xu et al. (2017) and show a general increase in precipitation, particularly in the central Pacific, however CP events look quite different. This is likely due to the definitions used by Xu et al. (2017) where they define EP events as the first empirical orthogonal function (EOF1) in tropical Pacific and CP as second empirical orthogonal function (EOF2). Other studies have, however, suggested that it is the combination of EOF1 and EOF2 that should be used to identify EP and CP events (Takahashi et al., 2011). When comparing CMIP5 projections from Power et al. (2013), who also look at EOF1, some similarities are found for precipitation projections, but SST projections look quite different. These results likely differ both due to different definitions of event types as well as the different set of models used and differences between single model realisations and SMILEs. We note that we also consider extreme El Niños, and discuss results for this event type in Supplementary Information 4: Extreme Niños.

4   Summary and Conclusions

In this study we use supervised machine learning combined with observed SST products to develop a new classifier for ENSO events, which classifies events into La Niña, neutral, Eastern Pacific (EP) El Niño, and Central Pacific (CP) El Niño. This method uses differences in the pattern, amplitude, and evolution of events to make the classification. Using supervised machine

learning has the advantage that it includes spatial and temporal information from 18 SST products to classify events without relying on pre-defined metrics, individual parameters, or manual identification. We then apply this classifier to seven SMILEs to identify ENSO events similar to those observed. By using SMILEs we examine forced changes in ENSO compared to the magnitude of internal variability. We find that:

1. All SMILEs bar CSIRO capture the observed pattern, evolution, frequency, and pattern correlation of EP and CP events, although known biases in the spatial pattern (e.g. SST anomalies located too far west) are found.

2. The observed increase in the frequency of CP events is within the range of the SMILEs internal variability for the period 1950 onwards, but not for the entire observed record.

3. CP El Niño frequency and amplitude are not projected to change in the future. EP El Niño frequency is projected to either increase or not change.

4. The SMILEs do not agree on projections of EP El Niño amplitude and La Niña frequency and amplitude. EP event amplitude projections are found to be weakly linked to changes in the zonal-mean gradient across the Pacific in 2 out of 5 models.

5. Models show differences in projected patterns of ENSO SST and precipitation that do not seem to be simply linked to the tropical Pacific mean state changes. However, the precipitation and SST changes in individual models are linked.

In conclusion, supervised machine learning has been used to build a new ENSO classifier for climate models that takes into account SST evolution along the tropical Pacific, and can be used to identify events that behave similarly to those observed. Future work running all classification schemes on SMILEs and comparing this new supervised learning algorithm with other methods would be informative to compare the use of different classification schemes. We find that the models do not project changes in CP El Niño frequency or amplitude, project either no change or an increase in EP El Niño frequency, and demonstrate disparity in future changes in other event types, and in the projected spatial patterns of SST and precipitation. The large ensemble spread for frequency and amplitude highlights, similar to previous work, that SMILEs are needed to evaluate ENSO and make projections due to the large variability of ENSO characteristics on decadal and longer timescales.

References

An, S.-I. and Wang, B.: Interdecadal Change of the Structure of the ENSO Mode and Its Impact on the ENSO Frequency, Journal of Climate, 13, 2044 – 2055, https://doi.org/10.1175/1520-0442(2000)013<2044:ICOTSO>2.0.CO;2, 2000.

Ashok, K., Behera, S. K., Rao, S. A., Weng, H., and Yamagata, T.: El Niño Modoki and its possible teleconnection, Journal of Geophysical Research: Oceans, 112, https://doi.org/https://doi.org/10.1029/2006JC003798, 2007.

Barnes, E. A., Hurrell, J. W., Ebert-Uphoff, I., Anderson, C., and Anderson, D.: Viewing Forced Climate Patterns Through an AI Lens, Geophysical Research Letters, 46, 13 389–13 398, https://doi.org/https://doi.org/10.1029/2019GL084944, 2019.

Barnes, E. A., Toms, B., Hurrell, J. W., Ebert-Uphoff, I., Anderson, C., and Anderson, D.: Indicator Patterns of Forced Change Learned by an Artificial Neural Network, Journal of Advances in Modeling Earth Systems, 12, https://doi.org/https://doi.org/10.1029/2020MS002195, 2020.

Bellenger, H., Guilyardi, E., Leloup, J., Lengaigne, M., and Vialard, J.: ENSO representation in climate models: from CMIP3 to CMIP5, Climate Dynamics, 42, 1999–2018, https://doi.org/10.1007/s00382-013-1783-z, 2014.

Beobide-Arsuaga, G., Bayr, T., Reintges, A., and Latif, M.: Uncertainty of ENSO-amplitude projections in CMIP5 and CMIP6 models, Climate Dynamics, https://doi.org/10.1007/s00382-021-05673-4, 2021.

Cai, W., Borlace, S., Lengaigne, M., van Rensch, P., Collins, M., Vecchi, G., Timmermann, A., Santoso, A., McPhaden, M. J., Wu, L., England, M. H., Wang, G., Guilyardi, E., and Jin, F.-F.: Increasing frequency of extreme El Niño events due to greenhouse warming, Nature Climate Change, 4, 111–116, https://doi.org/10.1038/nclimate2100, 2014.

Cai, W., Wang, G., Dewitte, B., Wu, L., Santoso, A., Takahashi, K., Yang, Y., Carréric, A., and McPhaden, M. J.: Increased variability of eastern Pacific El Niño under greenhouse warming, Nature, 564, 201–206, https://doi.org/10.1038/s41586-018-0776-9, 2018.

Cai, W., Santoso, A., Collins, M., Dewitte, B., Karamperidou, C., Kug, J.-S., Lengaigne, M., McPhaden, M. J., Stuecker, M. F., Taschetto, A. S., Timmermann, A., Wu, L., Yeh, S.-W., Wang, G., Ng, B., Jia, F., Yang, Y., Ying, J., Zheng, X.-T., Bayr, T., Brown, J. R., Capotondi, A., Cobb, K. M., Gan, B., Geng, T., Ham, Y.-G., Jin, F.-F., Jo, H.-S., Li, X., Lin, X., McGregor, S., Park, J.-H., Stein, K., Yang, K., Zhang, L., and Zhong, W.: Changing El Niño-Southern Oscillation in a warming climate, Nature Reviews Earth Environment, https://doi.org/10.1038/s43017-021-00199-z, 2021.

Capotondi, A., Wittenberg, A. T., Newman, M., Lorenzo, E. D., Yu, J.-Y., Braconnot, P., Cole, J., Dewitte, B., Giese, B., Guilyardi, E., Jin, F.-F., Karnauskas, K., Kirtman, B., Lee, T., Schneider, N., Xue, Y., and Yeh, S.-W.: Understanding ENSO Diversity, Bulletin of the American Meteorological Society, 96, 921 – 938, https://doi.org/10.1175/BAMS-D-13-00117.1, 2015.

Capotondi, A., Wittenberg, A. T., Kug, J.-S., Takahashi, K., and McPhaden, M. J.: ENSO Diversity, chap. 4, pp. 65–86, American Geophysical Union (AGU), https://doi.org/https://doi.org/10.1002/9781119548164.ch4, 2020.

Chen, C., Cane, M. A., Wittenberg, A. T., and Chen, D.: ENSO in the CMIP5 Simulations: Life Cycles, Diversity, and Responses to Climate Change, Journal of Climate, 30, 775–801, https://www.jstor.org/stable/26387513, 2017a.

Chen, L., Li, T., Yu, Y., and Behera, S. K.: A possible explanation for the divergent projection of ENSO amplitude change under global warming, Climate Dynamics, 49, 3799–3811, https://doi.org/10.1007/s00382-017-3544-x, 2017b.

Chung, C. T. Y., Power, S. B., Arblaster, J. M., Rashid, H. A., and Roff, G. L.: Nonlinear precipitation response to El Niño and global warming in the Indo-Pacific, Climate Dynamics, 42, 1837–1856, https://doi.org/10.1007/s00382-013-1892-8, 2014.

Deser, C., Phillips, A. S., and Alexander, M. A.: Twentieth century tropical sea surface temperature trends revisited, Geophysical Research Letters, 37, https://doi.org/https://doi.org/10.1029/2010GL043321, 2010.

Dieppois, B., Capotondi, A., Pohl, B., Chun, K. P., Monerie, P.-A., and Eden, J.: ENSO diversity shows robust decadal variations that must

430   be captured for accurate future projections, Communications Earth & Environment, 2, 212, https://doi.org/10.1038/s43247-021-00285-6, 2021.

Fang, S.-W. and Yu, J.-Y.: Contrasting Transition Complexity Between El Niño and La Niña: Observations and CMIP5/6 Models, Geophysical Research Letters, 47, 2020GL088 926, https://doi.org/https://doi.org/10.1029/2020GL088926, 2020.

Feng, J., Lian, T., Ying, J., Li, J., and Li, G.: Do CMIP5 Models Show El Niño Diversity?, Journal of Climate, 33, 1619 – 1641,

435   https://doi.org/10.1175/JCLI-D-18-0854.1, 2020.

Fredriksen, H.-B., Berner, J., Subramanian, A. C., and Capotondi, A.: How Does El Niño–Southern Oscillation Change Under Global Warming—A First Look at CMIP6, Geophysical Research Letters, 47, e2020GL090 640, https://doi.org/https://doi.org/10.1029/2020GL090640, 2020.

Freund, M. B., Henley, B. J., Karoly, D. J., McGregor, H. V., Abram, N. J., and Dommenget, D.: Higher frequency of Central Pacific El Niño

440   events in recent decades relative to past centuries, Nature Geoscience, 12, 450–455, https://doi.org/10.1038/s41561-019-0353-3, 2019.

Giese, B. S. and Ray, S.: El Niño variability in simple ocean data assimilation (SODA), 1871–2008, Journal of Geophysical Research: Oceans, 116, https://doi.org/https://doi.org/10.1029/2010JC006695, 2011.

Gil, Y., Pierce, S. A., Babaie, H., Banerjee, A., Borne, K., Bust, G., Cheatham, M., Ebert-Uphoff, I., Gomes, C., Hill, M., Horel, J., Hsu, L., Kinter, J., Knoblock, C., Krum, D., Kumar, V., Lermusiaux, P., Liu, Y., North, C., Pankratius, V., Peters, S., Plale, B., Pope, A., Ravela,

445   S., Restrepo, J., Ridley, A., Samet, H., Shekhar, S., Skinner, K., Smyth, P., Tikoff, B., Yarmey, L., and Zhang, J.: Intelligent Systems for Geosciences: An Essential Research Agenda, Commun. ACM, 62, 76–84, https://doi.org/10.1145/3192335, 2018.

Guo, Y., Cao, X., Liu, B., and Peng, K.: El Niño Index Prediction Using Deep Learning with Ensemble Empirical Mode Decomposition, Symmetry, 12, https://doi.org/10.3390/sym12060893, 2020.

Ham, Y.-G., Jeong, Y., and Kug, J.-S.: Changes in Independency between Two Types of El Niño Events under a Greenhouse Warming

450   Scenario in CMIP5 Models, Journal of Climate, 28, 7561 – 7575, https://doi.org/10.1175/JCLI-D-14-00721.1, 2015.

Ham, Y.-G., Kim, J.-H., and Luo, J.-J.: Deep learning for multi-year ENSO forecasts, Nature, 573, 568–572, https://doi.org/10.1038/s41586-019-1559-7, 2019.

Haszpra, T., Herein, M., and Bódai, T.: Investigating ENSO and its teleconnections under climate change in an ensemble view – a new perspective, Earth System Dynamics, 11, 267–280, https://doi.org/10.5194/esd-11-267-2020, 2020.

455   Hendon, H. H., Lim, E., Wang, G., Alves, O., and Hudson, D.: Prospects for predicting two flavors of El Niño, Geophysical Research Letters, 36, https://doi.org/https://doi.org/10.1029/2009GL040100, 2009.

Hu, Z.-Z., Kumar, A., Ren, H.-L., Wang, H., L'Heureux, M., and Jin, F.-F.: Weakened Interannual Variability in the Tropical Pacific Ocean since 2000, Journal of Climate, 26, 2601 – 2613, https://doi.org/10.1175/JCLI-D-12-00265.1, 2013.

Huang, B., Angel, W., Boyer, T., Cheng, L., Chepurin, G., Freeman, E., Liu, C., and Zhang, H.-M.: Evaluating SST Analyses with Indepen-

460   dent Ocean Profile Observations, Journal of Climate, 31, 5015–5030, https://doi.org/10.1175/JCLI-D-17-0824.1, 2018.

Huang, P. and Xie, S.-P.: Mechanisms of change in ENSO-induced tropical Pacific rainfall variability in a warming climate, Nature Geoscience, 8, 922–926, https://doi.org/10.1038/ngeo2571, 2015.

Johnson, N. C.: How Many ENSO Flavors Can We Distinguish?, Journal of Climate, 26, 4816 – 4827, https://doi.org/10.1175/JCLI-D-12-00649.1, 2013.

465   Kao, H.-Y. and Yu, J.-Y.: Contrasting Eastern-Pacific and Central-Pacific Types of ENSO, Journal of Climate, 22, 615 – 632, https://doi.org/10.1175/2008JCLI2309.1, 2009.

Karamperidou, C., Jin, F.-F., and Conroy, J. L.: The importance of ENSO nonlinearities in tropical pacific response to external forcing, Climate Dynamics, 49, 2695–2704, https://doi.org/10.1007/s00382-016-3475-y, 2017.

Karpatne, A., Ebert-Uphoff, I., Ravela, S., Babaie, H. A., and Kumar, V.: Machine Learning for the Geosciences: Challenges and Opportunities, IEEE Transactions on Knowledge and Data Engineering, 31, 1544–1554, https://doi.org/10.1109/TKDE.2018.2861006, 2019.

Kim, H.-M., webster, J., and J.A., C.: Impact of Shifting Patterns of Pacific Ocean Warming on North Atlantic Tropical Cyclones, SCience, 325, 77–80, https://doi.org/10.1126/science.1174062, 2009.

Kim, S. T., Cai, W., Jin, F.-F., Santoso, A., Wu, L., Guilyardi, E., and An, S.-I.: Response of El Niño sea surface temperature variability to greenhouse warming, Nature Climate Change, 4, 786–790, https://doi.org/10.1038/nclimate2326, 2014.

Knutson, T. R., Manabe, S., and Gu, D.: Simulated ENSO in a Global Coupled Ocean–Atmosphere Model: Multidecadal Amplitude Modulation and CO2 Sensitivity, Journal of Climate, 10, 138 – 161, https://doi.org/10.1175/1520-0442(1997)010<0138:SEIAGC>2.0.CO;2, 1997.

Kohyama, T., Hartmann, D. L., and Battisti, D. S.: La Niña–like Mean-State Response to Global Warming and Potential Oceanic Roles, Journal of Climate, 30, 4207 – 4225, https://doi.org/10.1175/JCLI-D-16-0441.1, 2017.

Kug, J.-S., Jin, F.-F., and An, S.-I.: Two Types of El Niño Events: Cold Tongue El Niño and Warm Pool El Niño, Journal of Climate, 22, 1499 – 1515, https://doi.org/10.1175/2008JCLI2624.1, 2009.

Lemmon, D. E. and Karnauskas, K. B.: A metric for quantifying El Niño pattern diversity with implications for ENSO-mean state interaction, Climate Dynamics, 52, 7511–7523, https://doi.org/10.1007/s00382-018-4194-3, 2019.

Liu, Y., Cobb, K. M., Song, H., Li, Q., Li, C.-Y., Nakatsuka, T., An, Z., Zhou, W., Cai, Q., Li, J., Leavitt, S. W., Sun, C., Mei, R., Shen, C.-C., Chan, M.-H., Sun, J., Yan, L., Lei, Y., Ma, Y., Li, X., Chen, D., and Linderholm, H. W.: Recent enhancement of central Pacific El Niño variability relative to last eight centuries, Nature Communications, 8, 15 386, https://doi.org/10.1038/ncomms15386, 2017.

Maher, N., Matei, D., Milinski, S., and Marotzke, J.: ENSO Change in Climate Projections: Forced Response or Internal Variability?, Geophysical Research Letters, 45, 11,390–11,398, https://doi.org/10.1029/2018GL079764, 2018.

Maher, N., Power, S., and Marotzke, J.: More accurate quantification of model-to-model agreement in externally forced climatic responses over the coming century, Nature Communications, 12, https://doi.org/10.1038/s41467-020-20635-w, 2021.

McPhaden, M. J., Lee, T., and McClurg, D.: El Niño and its relationship to changing background conditions in the tropical Pacific Ocean, Geophysical Research Letters, 38, https://doi.org/https://doi.org/10.1029/2011GL048275, 2011.

Milinski, S., Maher, N., and Olonscheck, D.: How large does a large ensemble need to be?, Earth System Dynamics, 11, 885–901, https://doi.org/10.5194/esd-11-885-2020, 2020, 2020.

Newman, M., Shin, S.-I., and Alexander, M. A.: Natural variation in ENSO flavors, Geophysical Research Letters, 38, https://doi.org/https://doi.org/10.1029/2011GL047658, 2011.

Ng, B., Cai, W., Cowan, T., and Bi, D.: Impacts of Low-Frequency Internal Climate Variability and Greenhouse Warming on El Niño–Southern Oscillation, Journal of Climate, 34, 2205 – 2218, https://doi.org/10.1175/JCLI-D-20-0232.1, 2021.

Pascolini-Campbell, M., Zanchettin, D., Bothe, O., Timmreck, C., Matei, D., Jungclaus, J. H., and Graf, H.-F.: Toward a record of Central Pacific El Niño events since 1880, Theoretical and Applied Climatology, 119, 379–389, https://doi.org/10.1007/s00704-014-1114-2, 2015.

Pedregosa, F., Varoquaux, G., Gramfort, A., Michel, V., Thirion, B., Grisel, O., Blondel, M., Prettenhofer, P., Weiss, R., Dubourg, V., Vanderplas, J., Passos, A., Cournapeau, D., Brucher, M., Perrot, M., and Duchesnay, E.: Scikit-learn: Machine Learning in Python, Journal of Machine Learning Research, 12, 2825–2830, 2011.

Planton, Y. Y., Guilyardi, E., Wittenberg, A. T., Lee, J., Gleckler, P. J., Bayr, T., McGregor, S., McPhaden, M. J., Power, S., Roehrig, R., Vialard, J., and Voldoire, A.: Evaluating Climate Models with the CLIVAR 2020 ENSO Metrics Package, Bulletin of the American Meteorological Society, 102, E193 – E217, https://doi.org/10.1175/BAMS-D-19-0337.1, 2021.

Power, S., Delage, F., Chung, C., Kociuba, G., and Keay, K.: Robust twenty-first-century projections of El Niño and related precipitation variability., Nature, 502, 541–545, https://doi.org/10.1038/nature12580, 2013.

Rasmusson, E. M. and Carpenter, T. H.: Variations in Tropical Sea Surface Temperature and Surface Wind Fields Associated with the Southern Oscillation/El Niño, Monthly Weather Review, 110, 354 – 384, https://doi.org/10.1175/1520-0493(1982)110<0354:VITSST>2.0.CO;2, 1982.

Reichstein, M., Camps-Valls, G., Stevens, B., Jung, M., Denzler, J., Carvalhais, N., and Prabhat: Deep learning and process understanding for data-driven Earth system science, Nature, 566, 195–204, https://doi.org/10.1038/s41586-019-0912-1, 2019.

Ren, H.-L. and Jin, F.-F.: Niño indices for two types of ENSO, Geophysical Research Letters, 38, https://doi.org/https://doi.org/10.1029/2010GL046031, 2011.

Takahashi, K., Montecinos, A., Goubanova, K., and Dewitte, B.: ENSO regimes: Reinterpreting the canonical and Modoki El Niño, Geophysical Research Letters, 38, https://doi.org/https://doi.org/10.1029/2011GL047364, 2011.

Timmermann, A., An, S.-I., Kug, J.-S., Jin, F.-F., Cai, W., Capotondi, A., Cobb, K. M., Lengaigne, M., McPhaden, M. J., Stuecker, M. F., Stein, K., Wittenberg, A. T., Yun, K.-S., Bayr, T., Chen, H.-C., Chikamoto, Y., Dewitte, B., Dommenget, D., Grothe, P., Guilyardi, E., Ham, Y.-G., Hayashi, M., Ineson, S., Kang, D., Kim, S., Kim, W., Lee, J.-Y., Li, T., Luo, J.-J., McGregor, S., Planton, Y., Power, S., Rashid, H., Ren, H.-L., Santoso, A., Takahashi, K., Todd, A., Wang, G., Wang, G., Xie, R., Yang, W.-H., Yeh, S.-W., Yoon, J., Zeller, E., and Zhang, X.: El Niño-Southern Oscillation complexity, Nature, 559, 535–545, https://doi.org/10.1038/s41586-018-0252-6, 2018.

Toms, B. A., Barnes, E. A., and Ebert-Uphoff, I.: Physically Interpretable Neural Networks for the Geosciences: Applications to Earth System Variability, Journal of Advances in Modeling Earth Systems, 12, e2019MS002 002, https://doi.org/https://doi.org/10.1029/2019MS002002, 2020.

Tseng, Y.-h., Huang, J.-H., and Chen, H.-C.: Improving the Predictability of Two Types of ENSO by the Characteristics of Extratropical Precursors, Geophysical Research Letters, 49, e2021GL097 190, https://doi.org/https://doi.org/10.1029/2021GL097190, 2022.

Wang, B., Luo, X., Yang, Y.-M., Sun, W., Cane, M. A., Cai, W., Yeh, S.-W., and Liu, J.: Historical change of El Niño properties sheds light on future changes of extreme El Niño, Proceedings of the National Academy of Sciences, 116, 22 512–22 517, https://doi.org/10.1073/pnas.1911130116, 2019.

Watanabe, M., Kamae, Y., and Kimoto, M.: Robust increase of the equatorial Pacific rainfall and its variability in a warmed climate, Geophys. Res. Lett., 41, 3227–3232, https://doi.org/10.1002/2014GL059692, 2014.

Wittenberg, A. T.: Are historical records sufficient to constrain ENSO simulations?, Geophysical Research Letters, 36, https://doi.org/10.1029/2009GL038710, 2009.

Xu, K., Tam, C.-Y., Zhu, C., Liu, B., and Wang, W.: CMIP5 Projections of Two Types of El Niño and Their Related Tropical Precipitation in the Twenty-First Century, Journal of Climate, 30, 849 – 864, https://doi.org/10.1175/JCLI-D-16-0413.1, 2017.

Yeh, S.-W., Kug, J.-S., Dewitte, B., Kwon, M.-H., and Kirtman, B. P. Jin, F.-F.: El Niño in a changing climate, Nature, 461, 511–514, https://doi.org/10.1038/nature08316, 2009.

Yeh, S.-W., Kirtman, B. P., Kug, J.-S., Park, W., and Latif, M.: Natural variability of the central Pacific El Niño event on multi-centennial timescales, Geophysical Research Letters, 38, https://doi.org/https://doi.org/10.1029/2010GL045886, 2011.

Yeh, S.-W., Kug, J.-S., and S-I., A.: Recent progress on two types of El Niño: Observations, dynamics, and future changes, Asia-Pacific Journal of Atmospheric Sciences, 50, 69–81, https://doi.org/10.1007/s13143-014-0028-3, 2014.

Yu, J.-Y. and Fang, S.-W.: The Distinct Contributions of the Seasonal Footprinting and Charged-Discharged Mechanisms to ENSO Complexity, Geophysical Research Letters, 45, 6611–6618, https://doi.org/https://doi.org/10.1029/2018GL077664, 2018.

545 Yu, J.-Y. and Kim, S. T.: Identification of Central-Pacific and Eastern-Pacific types of ENSO in CMIP3 models, Geophysical Research Letters, 37, https://doi.org/https://doi.org/10.1029/2010GL044082, 2010.

Yun, K.-S., Lee, J.-Y., Timmermann, A., Stein, K., Stuecker, M. F., Fyfe, J. C., and Chung, E.-S.: Increasing ENSO-rainfall variability due to changes in future tropical temperature-rainfall relationship, Communications Earth Environment, 2, 43, https://doi.org/10.1038/s43247-021-00108-8, 2021.

550 Zheng, X.-T., Hui, C., and Yeh, S.-W.: Response of ENSO amplitude to global warming in CESM large ensemble: uncertainty due to internal variability, Climate Dynamics, pp. 1–17, https://doi.org/10.1007/s00382-017-3859-7, 2017.

Table 1. Years which are defined as Central Pacific (CP) and Eastern Pacific (EP) El Niños, La Niñas (LE), and Neutral (NE) events in the observational data. These years are found using Pascolini-Campbell et al. (2015) for CP years, https://psl.noaa.gov/enso/past-events.hptp for events 1896-2014 and https://origin.cpc.ncep.noaa.gov/products/analysis_monitoring/ensostuff/ONI_v5.php for events 2014-2019, and https://www.pmel.noaa.gov/tao/drupal/disdel/ to determine whether the 2019 El Niño was a CP event

| event type (total no. events)	years (starting year)
CP (14)	1914, 1940, 1958, 1963, 1968, 1977, 1986, 1990, 1991, 1994, 2002, 2003, 2004, 2019
EP (20)	1896, 1899, 1902, 1905, 1918, 1925, 1930, 1941, 1957, 1965, 1972, 1979, 1982, 1987, 1997, 2006, 2009, 2014, 2015, 2018
LN (26)	1903, 1908, 1909, 1910, 1916, 1917, 1924, 1933, 1938, 1942, 1949, 1950, 1954, 1955, 1961, 1970, 1973, 1975, 1988, 1998, 1999, 2007, 2010, 2011, 2016, 2017
NE (64)	all others between 1896-2019
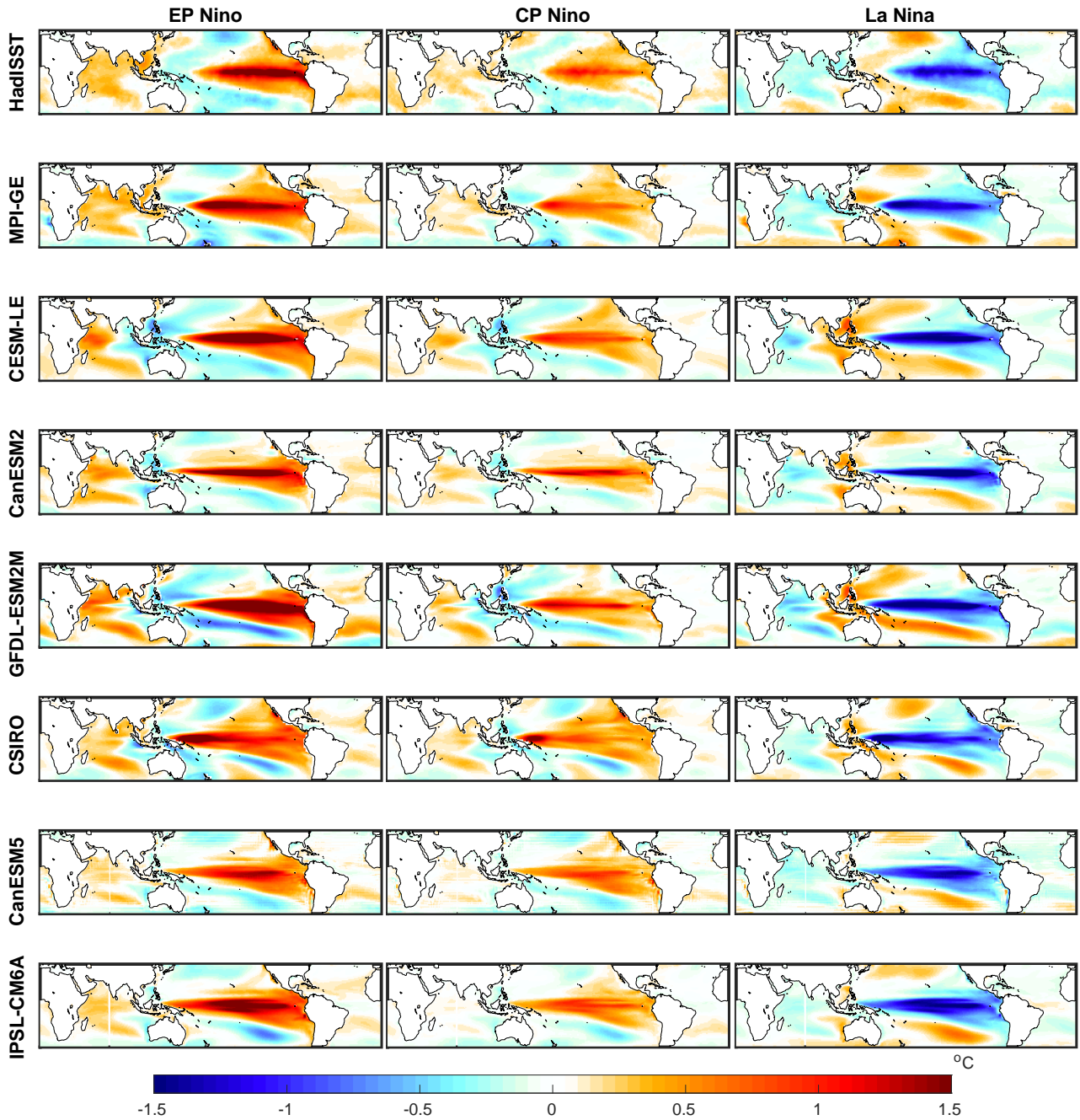
Figure 1. SST pattern for composites of EP and CP El Niños, and La Niña events (left, middle and right columns respectively). Shown for HadISST observations (top row) and each individual SMILE (in order of appearance; MPI-GE, CESM-LE, CanESM2, GFDL-ESM2M, CSIRO, CanESM5 and IPSL-CM6A). The SST pattern is shown for the November, December, January average. SMILE data has the forced response (ensemble mean) removed prior to calculation, HadISST is detrended using a second order polynomial then each months average is removed. The time period used is all of the historical, which is shown for the observations in Table S1 and SMILEs in Table S2.

Table 2. Scores for different algorithms tested. Scores are defined in section 2.2. Details on the tuning of the hyper-parameters can be found on https://github.com/nicolamaher/classification

Algorithm (python name)	tuned hyper-parameters	Accuracy	CVS	P-CP	P-EP	P-LN	P-NE	R-CP	R-EP	R-LN	R-NE
(1) NearestNeighbours (KNeighborsClassifier)	n neighbors=1	0.96	0.94	1	1	1	0.93	0.92	1	0.85	1
(5) NeuralNet (MLPClassifier)	hidden layers=500 max iterations= 1500 alpha= 0.01	0.96	0.93	1	1	1	0.93	1	0.95	0.84	1
(9) RandomForest (RandomForestClassifier)	max depth = 100	0.91	0.91	0.9	0.96	1	0.88	0.84	0.92	0.75	0.99
FINAL: ensemble classifier (VotingClassifier)	Soft vote (1,5,9)	0.96	0.95	1	1	1	0.93	0.92	1	0.85	1

Table 3. Scores for the final ensemble classifier. Test 1 uses all available data, with HadISST kept aside for testing. Test 2 uses the longer datasets, ERSST, COBE, Kaplan and HadISST for training and testing. The data is split so that the augmented events must all occur in the same section of the data (i.e. training or testing). The data split is randomly completed 10 times on alternative splits of the training and testing data. To complete this we use the python function *train test split*. Test2 w/check again uses the same function, however 10 data splits are manually chosen to ensure that they sample events from across the time-dimension and have a reasonable amount of each type of event. Test2 w/check HadISST uses the same splits as Test2 w/check, but only uses HadISST for training and testing.

Test	Min/Max score	Accuracy	CVS	P-CP	P-EP	P-LN	P-NE	R-CP	R-EP	R-LN	R-NE
Test 1		0.96	0.95	1	1	1	0.92	0.92	1	0.85	1
Test 2 random	Min	0.65	0.96	0.32	0.36	0.6	0.68	0.14	0.79	0.66	0.74
	Mean	0.77	0.97	0.78	0.62	0.8	0.82	0.53	0.89	0.78	0.81
	Max	0.84	0.98	1	0.88	0.94	0.96	0.93	1	0.93	0.9
Test 2 w/check	Min	0.66	0.97	0.52	0.57	0.44	0.65	0.43	0.63	0.6	0.66
	Mean	0.76	0.97	0.75	0.74	0.79	0.76	0.64	0.8	0.72	0.8
	Max	0.86	0.98	0.95	0.92	0.97	0.84	0.95	1	0.94	0.95
Test 2 w/check HadISST only	Min	0.58	0.66	0.25	0.45	0.5	0.54	0.25	0.57	0.5	0.58
	Mean	0.74	0.73	0.65	0.81	0.8	0.73	0.5	0.8	0.66	0.82
	Max	0.9	0.77	1	1	1	0.84	1	1	0.86	1

Table 4. Frequency of events (as a percentage) in the historical period for observations (HadISST) and the SMILEs, as well as the correlation between EP and CP patterns. The mean frequency and correlation across each ensemble is shown with the minimum and maximum values in brackets. The time period used is all of the historical, which is shown for the observations in Table S1 and SMILEs in Table S2.

| Model	EP no ev	CP no ev	LN no ev	EP/CP corr
HadISST	16.1	11.2	21.0	0.85
MPI-GE	16.6 (11.0/21.3)	5.3 (1.3/11.6)	19.0 (11.0/23.9)	0.72 (0.47/0.88)
CESM-LE	22.0 (14.1/29.4)	5.5 (1.2/11.8)	23.9 (18.8/32.9)	0.72 (0.24/0.87)
CanESM2	19.5 (11.4/27.1)	8.8 (2.9/18.6)	23.3 (14.3/30)	0.78 (0.38/0.90)
GFDL-ESM2M	18.6 (10.9/23.6)	14.5 (7.3/23.6)	26.9 (18.2/36.4)	0.71 (0.54/0.88)
CSIRO	12.1 (9.0/16.1)	5.4 (1.3/8.4)	14.1 (8.4/18.7)	0.79 (0.59/0.89)
CanESM5	9.4 (4.9/12.8)	5.8 (3.0/10.4)	16.6 (10.4/22.6)	0.80 (0.67/0.89)
IPSL-CM6A	18.9 (14.6/23.8)	4.2 (1.2/9.1)	21.3 (17.7/25.6)	0.70 (0.43/0.86)
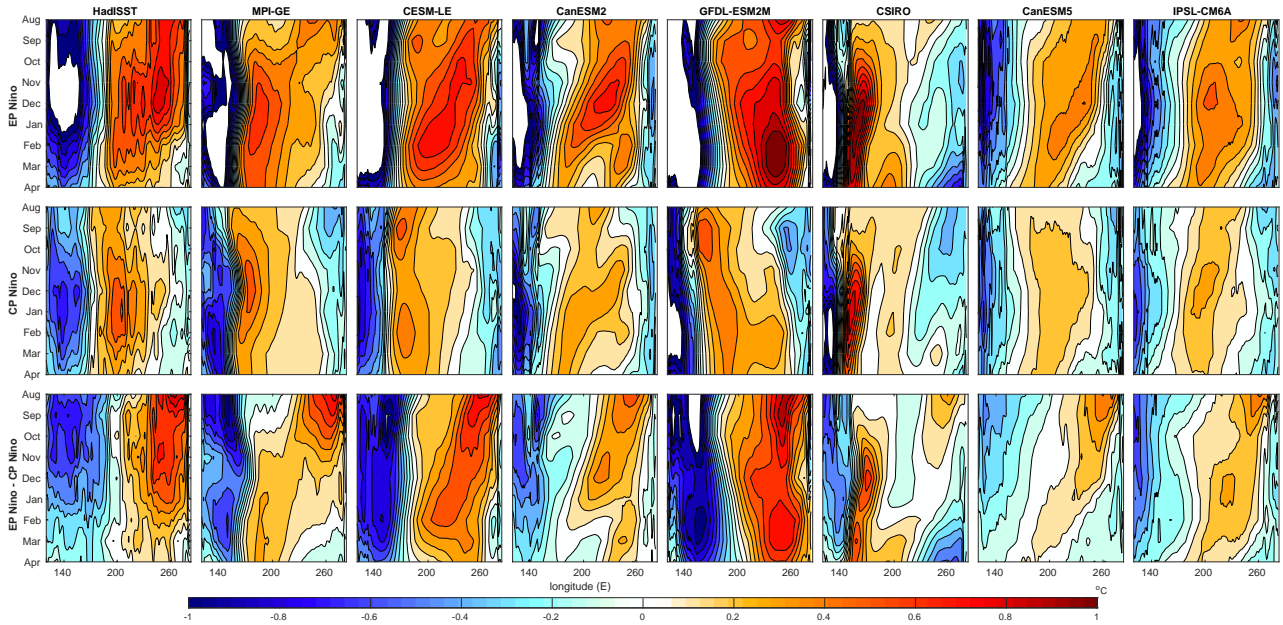
Figure 2. Hovmöller of relative SST along the equator in the Pacific Ocean for composites of EP and CP El Niños and EP minus CP El Niños (top, middle and bottom row respectively). Shown for HadISST observations (left column) and each individual SMILE (in order of appearance; MPI-GE, CESM-LE, CanESM2, GFDL-ESM2M, CSIRO, CanESM5 and IPSL-CM6A). SST is averaged between 5N and 5S and shown for August to April. SMILE data has the forced response (ensemble mean) removed prior to calculation, HadISST is detrended using a second order polynomial then each months average is removed. The time period used is all of the historical, which is shown for the observations in Table S1 and SMILEs in Table S2. Relative SST is calculated by removing the average SST between 120E and 280E individually for each month.
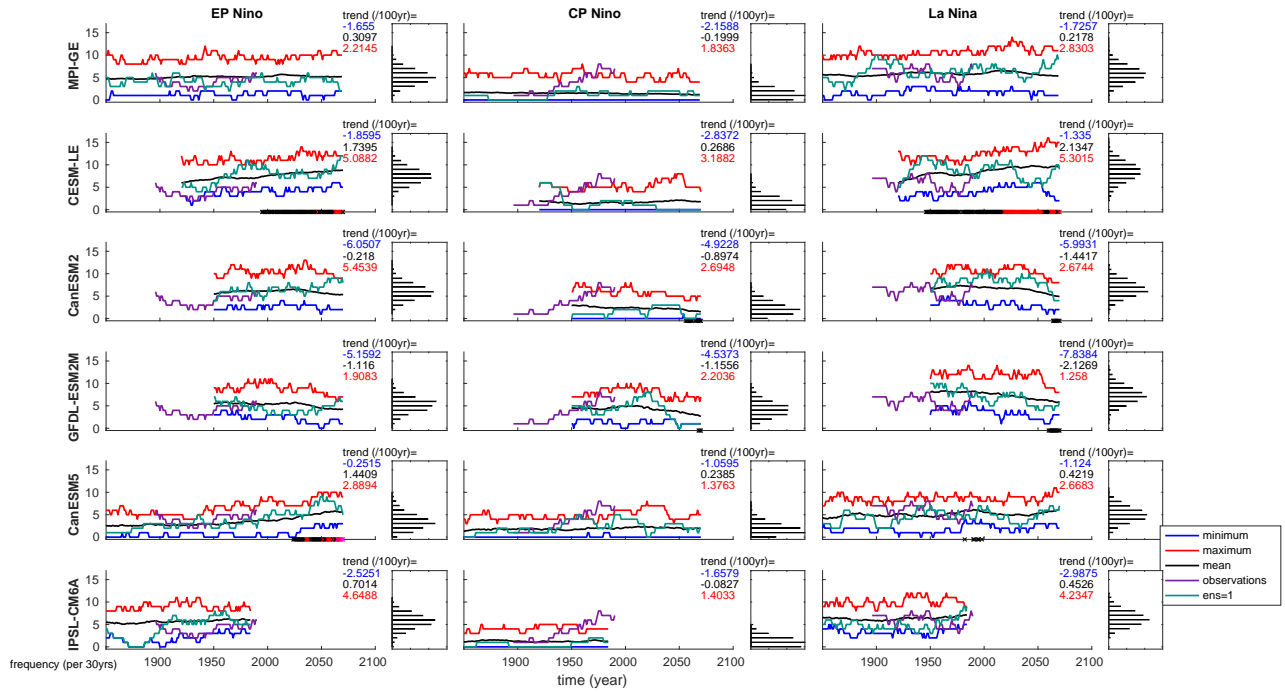
Figure 3. ENSO frequency in each SMILE for EP and CP El Niños, and La Niña events (left, middle and right columns respectively). Black line shows the ensemble mean for each year, red line shows the ensemble maximum, the blue line the ensemble minimum, the purple line is HadISST observations, and the green line is the first ensemble member. Frequency is calculated as the number of events in a single ensemble member per 30 years, taken as a running calculation along the time-series. PDFs show the distribution of ensemble members for the entire time-series. Black dots on the x-axis demonstrate when the signal (current ensemble mean minus the ensemble mean at the beginning of the time-series) is greater than the noise (standard deviation taken across the ensemble). Red dots show when the signal is 1.645 times the noise, while magenta dots show the same when the signal is greater than 2 times the noise. These thresholds correspond to the *likely*, *very likely* and *extremely likely* ranges. Maximum (red), mean (black) and minimum (blue) trends across the individual ensemble members are shown in text at the top right of each panel. We note that the trends are calculated over the entirety of the simulation length for each SMILE. This means that due to the different time periods covered, trends are not directly comparable between different SMILEs.
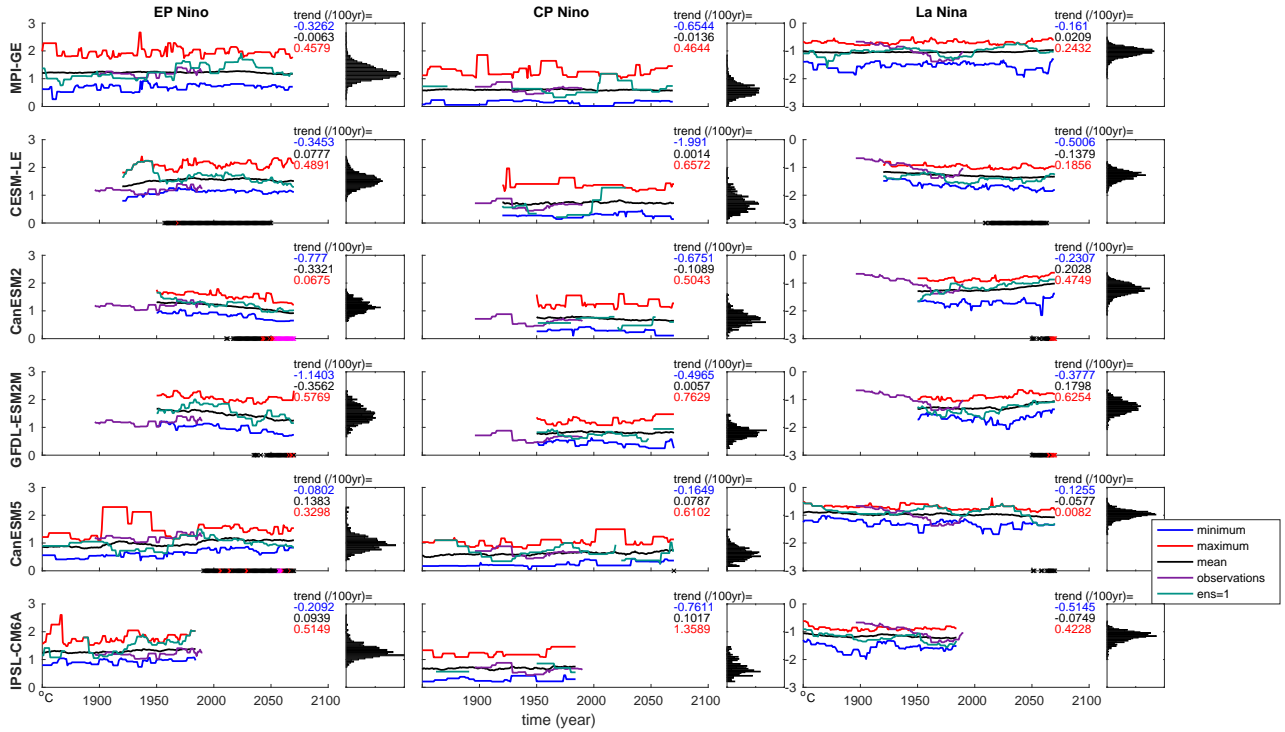
Figure 4. ENSO amplitude in each SMILE for EP and CP El Niños, and La Niña events (left, middle and right columns respectively). Black line shows the ensemble mean for each year, red line shows the ensemble maximum, the blue line the ensemble minimum, the purple line is HadISST observations, and the green line is the first ensemble member. Amplitude is calculated as the November, December, January mean for the region 160E to 80W between 5N and 5S after the ensemble mean has been removed for each event in a single ensemble member taken as a running calculation along the time-series for 30-year periods. PDFs show the distribution of ensemble members for the entire time-series. Black dots on the x-axis demonstrate when the signal (current ensemble mean minus the ensemble mean at the beginning of the time-series) is greater than the noise (standard deviation taken across the ensemble). Red dots show when the signal is 1.645 times the noise, while magenta dots show the same when the signal is greater than 2 times the noise. These thresholds correspond to the *likely*, *very likely* and *extremely likely* ranges. Maximum (red), mean (black) and minimum (blue) trends across the individual ensemble members are shown in text at the top right of each panel. We note that the trends are calculated over the entirety of the simulation length for each SMILE. This means that due to the different time periods covered, trends are not directly comparable between different SMILEs.
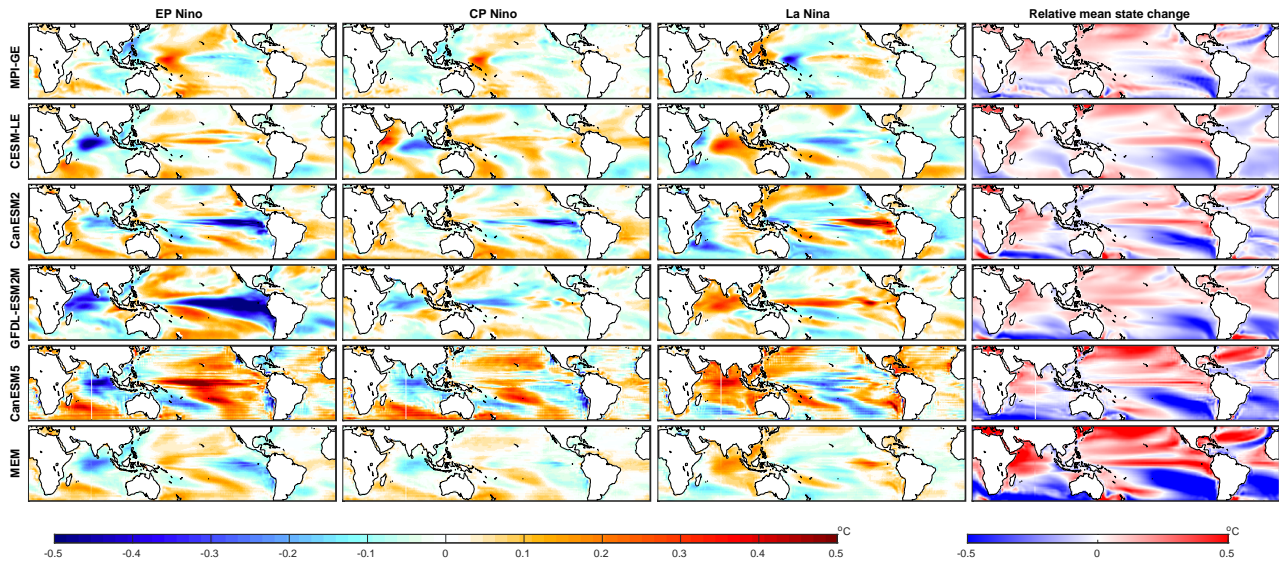
23

Figure 5. Change in SST pattern in each SMILE in the period 2050-2099 as compared to 1950-1999 for EP and CP El Niños, and La Niña events (left, centre left and centre right columns respectively. The mean state change in SST is shown in the right column. Shown for each individual SMILE (in order of appearance; MPI-GE, CESM-LE, CanESM2, GFDL-ESM2M, CanESM5) and the multi-ensemble mean (bottom row). The SST pattern is calculated as the November, December, January average and composited for each event type over each time-period. The relative mean state change is calculated as the ensemble mean SST over each time period, with the earlier period subtracted from the latter relative to the total change in the region shown (0-360E, 40S-40N). SMILE data has the forced response (ensemble mean) removed prior to calculation for the SST change, but not the mean state change.
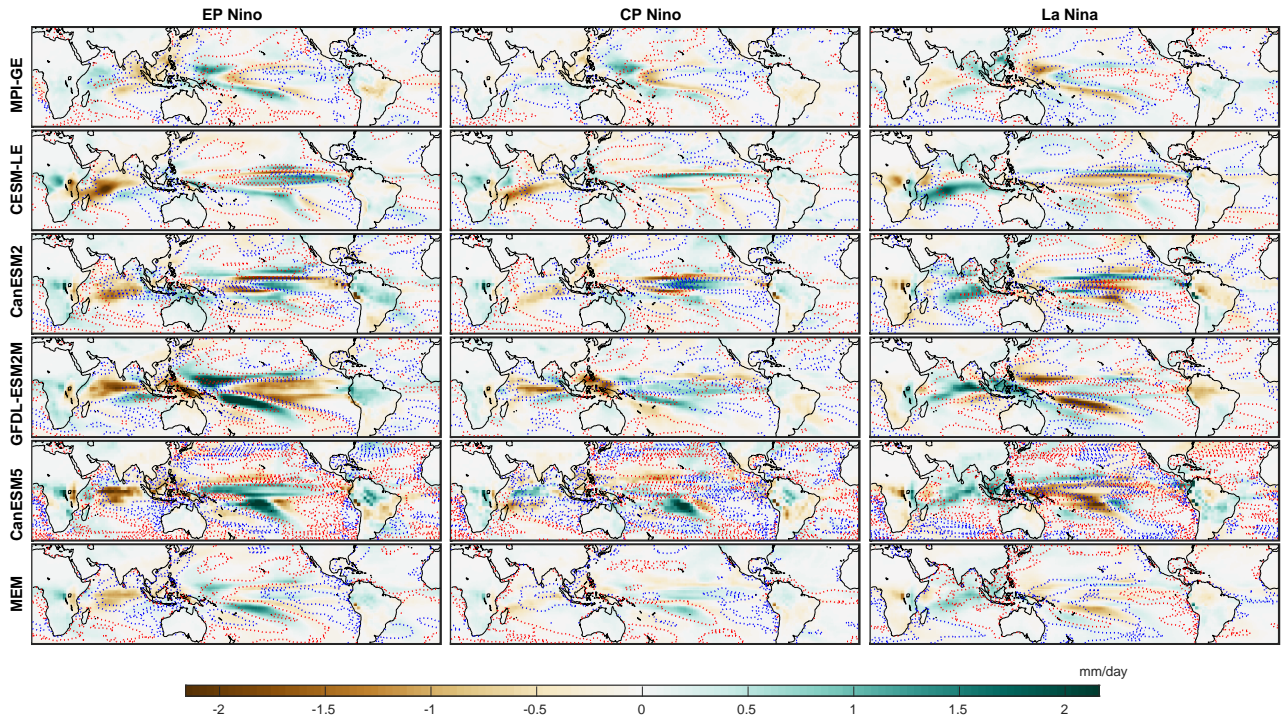
Figure 6. Change in precipitation pattern in each SMILE in the period 2050-2099 as compared to 1950-1999 for EP and CP El Niños, and La Niña events (left, middle and right columns respectively). The SST change from Figure 5 is shown as contours for reference (blue=cooling, red=warming). Shown for each individual SMILE (in order of appearance; MPI-GE, CESM-LE, CanESM2, GFDL-ESM2M, CanESM5) and the multi-ensemble mean (bottom row). The precipitation pattern is calculated as the November, December, January average and composited for each event type over each time-period. SMILE data has the forced response (ensemble mean) removed prior to calculation.